JOURNAL OF MATERIALS SCIENCE **36** (2001) 949–955

Preparation and characterization of the Sb-doped TiO_2 photocatalysts

JOOHO MOON*
Department of Ceramic Engineering, Yonsei University, Seoul 120-749, South Korea
E-mail: jmoon@yonsei.ac.kr

H. TAKAGI, Y. FUJISHIRO, M. AWANO
National Industrial Research Institute of Nagoya, Nagoya 462-8510, Japan

Doped TiO_2 photocatalysts have been prepared by a coprecipitation method. Uniformly doped nanocrystalline TiO_2 of 10–20 nm sizes was synthesized by calcinating the coprecipitated gels at 400–650°C. Photocatalytic characterization along with the microstructural investigation for each catalyst provides better understanding of the photocatalytic behavior. It was found that the photodegradation of methylene blue (MB) was a complex function of the doping type and its concentration and the microstructural characteristics of the catalysts. Antimony doing significantly improved photocatalytic performance as compared to the undoped TiO_2. Post-treatment of the as-precipitated wet doped Ti gels in an organic solvent also increased the surface area, forming approximately 8 nm size doped TiO_2 with surface area ~149 m^2/g. Superior catalytic activity was observed in the Sb-doped TiO_2 samples at a doping concentration ranging from 1 to 5 at%. Using the 5 at% Sb-doped TiO_2 catalyst treated in butanol, 100 ppm of MB could be decomposed completely within 1 h, which was better than the commercial Degussa P-25.

1. Introduction

Semiconductor photocatalysis is a promising technology that has a variety of applications in environmental systems such as air purification, water disinfection, hazardous waste remediation, and water purification [1, 2]. Several semiconductors have band gap energies sufficient for promoting or catalyzing a wide range of chemical reactions of environmental interest. Among many candidates, TiO_2 has proven to be the most suitable for widespread environmental applications because of its biological and chemical inertness, stability against photocorrosion and chemical corrosion, and cost-effectiveness [3].

Photoexcitation of TiO_2 with light of energy that matches its band gap yields electron-hole pairs. Photoproduced electrons and holes can migrate to the surface and react with adsorbed reactants in the desired redox process, or they may undergo undesired recombination, dissipating the input energy as heat. The photocatalytic efficiency depends on the competition between these two processes, i.e., the ratio of the surface charge carrier transfer rate to the electron-hole recombination rate. To increase the quantum yield, the photoinduced electrons and holes should be separated to suppress recombination by utilizing a suitable surface defect state as a temporal trap [4].

One of the effective methods to control surface properties of TiO_2 is to introduce defects into the lattice through selective metal ion doping [5–14]. Many transition metal ion dopants have been investigated for the TiO_2 system, among which Fe^{3+} has been most extensively examined. Understanding of the photocatalytic process, mechanism, and kinetics in the doped TiO_2 is complex, however, and requires a fundamental knowledge about physical chemistry of semiconductor-liquid interfaces and semiconductor physics. The photocatalytic behavior is even influenced by physicochemical variables of the catalysts including particle size, surface area, crystallinity and the state of surface hydration [15–17]. This complex phenomenology makes it difficult to draw unifying conclusions by direct comparisons between the studies, and often leads to a controversial issue.

In this study, nanocrystalline TiO_2 particles doped with antimony metal ion are synthesized. The photocatalytic behavior of the resulting powders is characterized by quantifying the degradation of an organic dye, methylene blue, in the aqeuous suspension. It was determined in the preliminary study that Sb was more photoactive for the degradation of methylene blue as compared to other dopants such as Cr, Fe, Nb, and Ta. The detailed microstructural characteristics for the Sb-doped TiO_2 catalyst system are investigated as a function of the doping content, the preparation method, and the calcination conditions.

* Author to whom all correspondence should be addressed.

2. Materials and methods

2.1. Catalyst preparation

Nanocrystalline TiO_2-based catalysts were prepared by coprecipitation from titanium tetrachloride. All chemicals used in this study were reagent-grade supplied from Wako Pure Chemical Industries. Firstly, $TiCl_4$ was mixed with HCl and deionized water to inhibit premature hydrolysis. Amorphous titanium hydrous gels were precipitated upon neutralization with NH_4OH at ~pH 8. Modification of pure TiO_2 was achieved by incorporation of metal cation at a doping level ranging from 0.25 to 10 nominal atomic % (at%). $SbCl_5$ was used as a precursor of the dopant. Metal salt was dissolved in nitric acid, followed by mixing with aqueous titanium tetrachloride solution under vigorous stirring at room temperature. Complex amorphous Ti gels were prepared through coprecipitation from homogeneous precursor solutions. The resulting precipitates were repeatedly washed to remove undesirable anions such as Cl^-, followed by drying at 120°C for 12 h. In some cases, the coprecipitated wet gels were treated in a butanol at 100°C for 3 h prior to the drying step. The dried precipitates were calcined at temperatures from 400–650°C in air. The calcined powders were ball-milled using ZrO_2 media in ethanol for 3 h prior to powder characterization.

2.2. Catalyst characterization

Powder X-ray diffraction (XRD, Phillips APD1700) was used for crystal phase identification and crystallite size estimation of each doped TiO_2. High-purity silicon powder (99.9999%) was used as an internal standard to determine normalized relative X-ray intensities for anatase and rutile and to account for instrumental line broadening effect during crystal size estimation. Particle morphologies of the doped TiO_2 were also examined by transmission electron microscopy (TEM, JEOL JEM-4000FX) at 400 KV. Surface area of the powders was determined by B.E.T. nitrogen adsorption techniques (Coulter, Omnisorp 360). Diffuse reflectance spectra were also obtained for the dry-pressed disk samples using a Uv-Vis-NIR spectrophotometer (JASCO V-570) equipped with an ISN-470 integrating sphere assembly. Reflectance spectra were referenced to $BaSO_4$.

2.3. Photoactivity measurement

The photocatalytic activity of each doped TiO_2 system was characterized in terms of the degradation of a cationic organic dye, methylene blue (MB). Methylene blue was selected because of its strong adsorption characteristics on metal oxide surfaces, well-defined optical absorption characteristics, and good resistance to light degradation, which makes easy its quantification [18]. 0.05 g of each catalyst was suspended in 20 ml of standard MB aqueous solution (100 ppm) using 30 ml-capacity Pyrex vials. The photocatalytic behavior of Degussa P-25 was also measured as a reference to compare with the synthesized catalysts. The catalysts were ultrasonically agitated for 10 min in MB solution in the absence of light to attain the equilibrium adsorption on the catalyst surface. The samples were then irradiated under stirring using a 500 W xenon arc lamp from which the light was collimated by a fused silica condenser lens. The wavelength selection was achieved with glass and water filters (330–600 nm, $\lambda_{max} = 500$ nm) and the radiation intensity was 0.8 W/cm^2 at a distance of 25 cm. After a given irradiation time, the catalysts were separated from the supernatant by centrifugation. A UV-vis spectrophotometer (Shimadzu UV-1600PC) was utilized to measure absorbances at 665 nm. The extent of MB photodecomposition was calculated using a calibrated relationship between the measured absorbance and its concentration. The measurements were repeated for each catalytic system, and the experimental error was found to be within ±1%. Approximately 10% MB was photodegraded in the absence of any catalyst under the same irradiation conditions. All the reported amounts of decomposition took into account this self-decomposition.

3. Results

3.1. Characterization of the doped TiO_2 powders

As-precipitated amorphous doped Ti gels undergo crystallization during calcination. Microstructural characteristics of the resulting calcined powders depend upon calcination temperature, synthesis procedure, and doping concentration. X-ray analysis indicated that all the Sb-doped TiO_2 powders did not exhibit any impurity phase, even at higher doping concentration (>5 at%) when calcined at 650°C. Similarly, energy-dispersive X-ray (EDX) analysis did not detect any other peaks except TiO_2, and confirmed uniform distribution of the doping element within its spot size ~10 nm for the aggregates of the powders. These results support that the current doping procedure allows intimate and uniform mixing of the dopants, forming stable solid solutions with TiO_2.

Doping TiO_2 with a foreign metal ion induces sluggish anatase-to-rutile phase transition compared with the undoped TiO_2 as shown in Table I. The 1 at% Sb-doped TiO_2 calcined at 600°C, 2 h showed pure anatase phase, while the undoped TiO_2 was a mixture of anatase and rutile. The doped TiO_2 powders also had smaller particle size and larger surface area than the pure TiO_2.

TABLE I Particle characteristics of the undoped and doped TiO_2

Sample ID	$I_{(Anatase)}/I_{Si}$	$I_{(Rutile)}/I_{Si}$	Fraction of rutile	Crystallite size (nm)	Surface area (m^2/g)
Undoped	1.44	0.03	0.029	21.39	55.9
1 at% Sb	2.18	0	0	14.83	68.6

All samples were calcined at 600°C, 2 h.

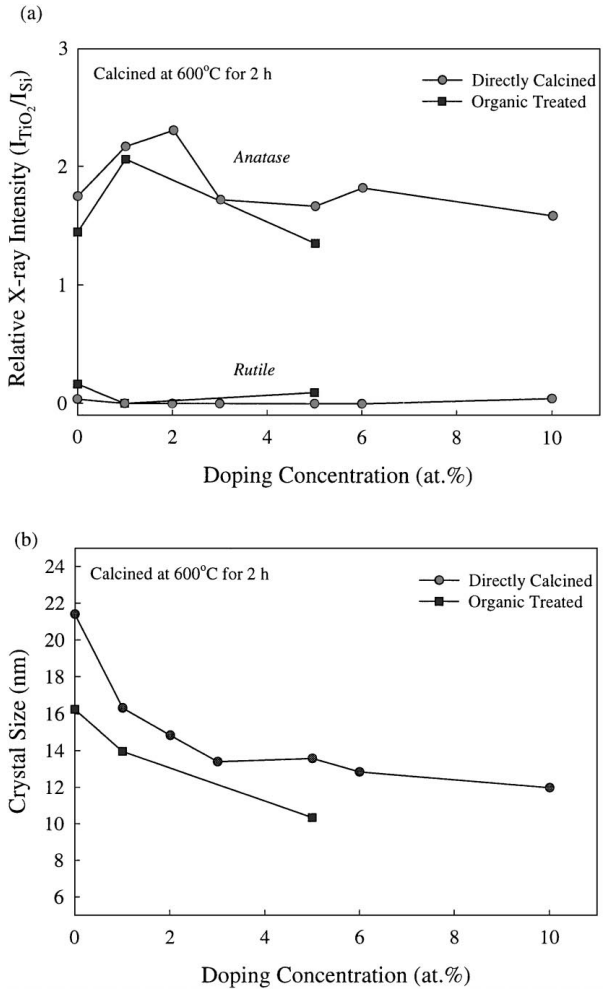

Figure 1 Variations of (a) the relative anatase and rutile X-ray intensities and (b) crystal size for the Sb-doped TiO_2 samples as a function of doping concentration and preparation method.

Doping concentration also influences the relative intensities of anatase and rutile observed in the doped TiO_2, as presented in Fig. 1. Crystallinity of the anatase phase for the Sb-doped TiO_2 calcined at 600°C was maximized at a concentration of 2 at% and then decreased again. Further doping above 5 at% did not bring about any noticeable variation in the degree of crystallization. However, the estimated crystal size monotonically decreased with increasing doping concentration from 21 to 12 nm.

Post-treatment in an organic solvent modifies the particle characteristics of the catalysts as summarized in Table II. All the Sb-doped TiO_2 treated in the butanol showed a lower degree of crystallization, an increased surface area, and a decreased particle size than the untreated counterparts. Doping content dependence of relative anatase-to-rutile ratio and crystal size was very similar to the directly calcined TiO_2, as seen in Fig. 1. The crystallinity of the anatase phase showed a maximum at 1 at% and the crystal size decreased with the increasing Sb content. It is believed that the organic solvent treatment enhances dehydration and terminates polymeric chain linkage in the amorphous gels. These surface modifications can prevent particle agglomeration, forming well-defined nanocrystalline powders with high surface area after calcination.

Fig. 2 shows TEM micrographs of nanocrystalline Sb-doped TiO_2 prepared by two different methods. The organic solvent treated 1 at% Sb-TiO_2 particles presented smaller particle size than the untreated counterpart. The average particle sizes of the 1 at% Sb doped TiO_2 calcined at 500°C, 2 h were approximately 13 nm for the picture (a) and 10 nm for the picture (b). These sizes are in reasonably well agreement with the values estimated by X-ray peak broadening.

Doping also modifies light absorption characteristics of TiO_2 as shown in Fig. 3. An abrupt increase in the absorption shortly after 400 nm can be assigned to the intrinsic band gap absorption of pure anatase TiO_2 (∼3.2 eV). It is apparent that the diffuse reflectance-spectra (DRS) of all the doped TiO_2 samples have increased absorbances in the visible range with a red shift in the band gap transition. The presence of Sb resulted in a higher absorption in the visible range. The onset of the absorption shifts to the red range with the increasing doping content. The organic solvent treated sample exhibited a similar reflectance spectrum as compared with the untreated counterpart, with a slightly higher absorption between 650–800 nm. Red shift associated with the present types of dopants can be attributed to a charge transfer transition between the metal ion d electrons and the TiO_2 conduction or valence band [8].

3.2. Characterization of photocatalytic activity

Fig. 4 shows photodecomposed MB (%) for the Sb-doped TiO_2 as a function of dopant concentrations. Doping of TiO_2 with Sb significantly enhances the photocatalytic efficiency as compared to the undoped TiO_2. The decomposition of MB rapidly increased

TABLE II Particle characteristics and photocatalytic activity of the various doped TiO_2 powders prepared by two different methods

Sample ID		$I_{(Anatase)}/I_{Si}$	Crystallite size (nm)	Surface area (m^2/g)	Decomposed MB (%)
Directly calcined	Undoped	2.08	14.1	60.3	70.1
	0.5 at% Sb	2.20	13.9	78.6	84.9
	1 at% Sb	1.67	13.7	80.4	88.0
	5 at% Sb	1.46	12.2	83.4	88.5
Organic solvent treated	Undoped	1.53	11.7	104.6	76.4
	0.5 at% Sb	1.72	11.5	107.0	94.4
	1 at% Sb	1.68	11.0	117.3	98.2
	5 at% Sb	0.84	8.50	149.2	98.4

All samples were calcined at 500°C, 2 h.

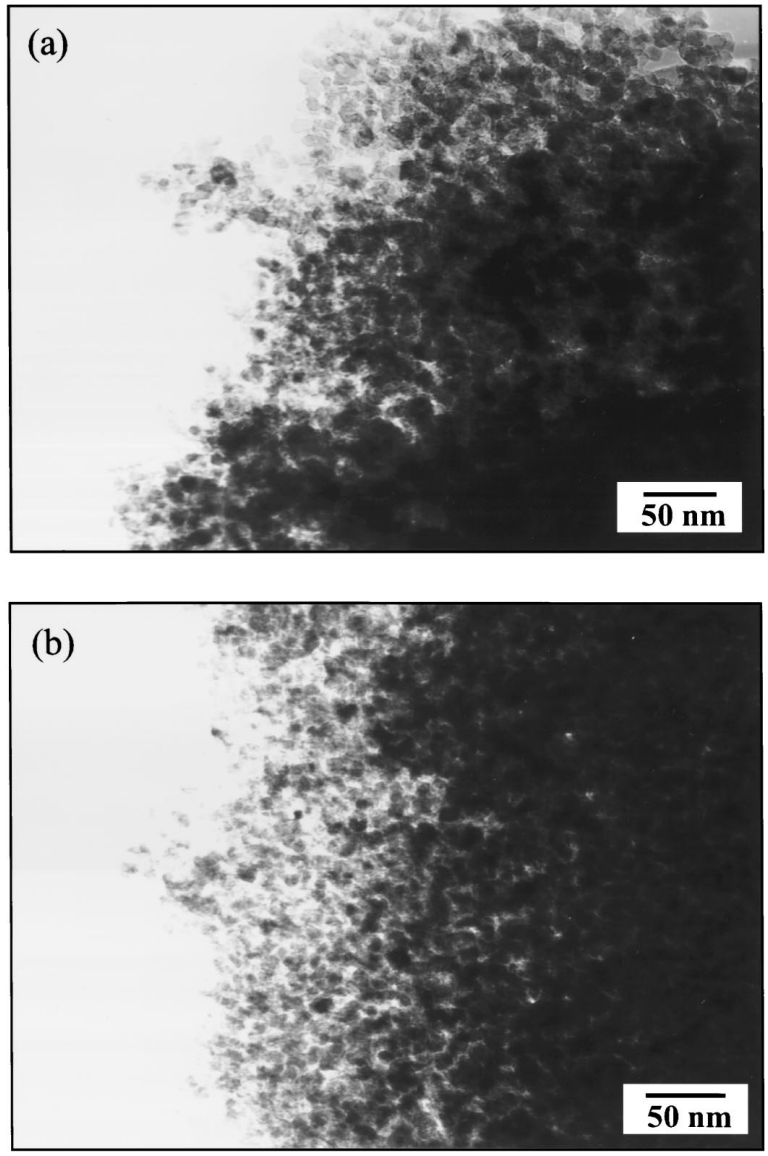

Figure 2 TEM micrographs showing nanocrystalline Sb-doped TiO_2: (a) the directly calcined 1 at% Sb-TiO_2 and (b) the organic solvent treated 1 at% Sb-TiO_2.

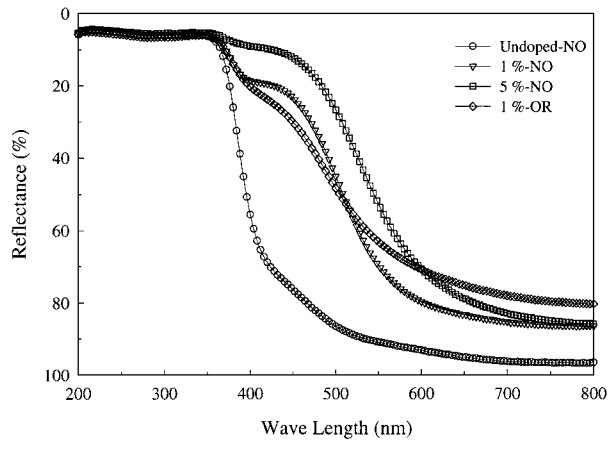

Figure 3 Diffuse reflectance spectra for the Sb-doped TiO_2 as a function of dopant content and preparation method. All the catalysts were calcined at 500°C for 2 h. 'NO' indicates the directly calcined samples, whereas 'OR' represents the organic solvent treated powder.

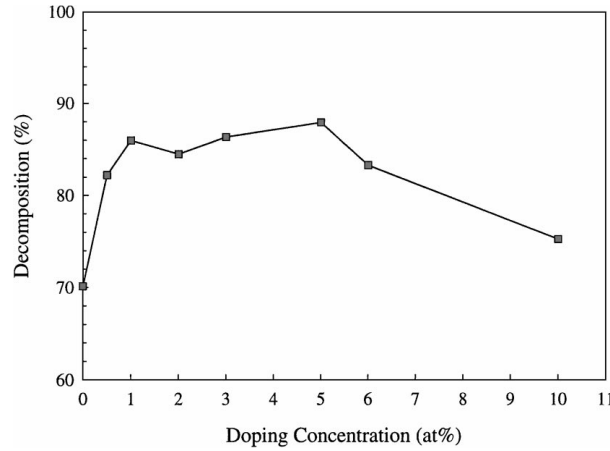

Figure 4 Photodegraded amounts of methylene blue by the Sb-doped TiO_2 as a function of doping concentration. All the catalysts were calcined at 500°C for 2 h. Irradiation time was 42 min.

with the increasing doping concentrations below 1 at%. The photocatalytic activities were high in the range of 1–5 at%, remaining unchanged within experimental deviations. However, a further increase in dopant content above 5 at% reduced the photocatalytic activity. Lower photoactivity for the doped TiO_2 with higher content may be associated with formation of a non-photoactive phase such as Sb_2O_4 on the surface of the powders

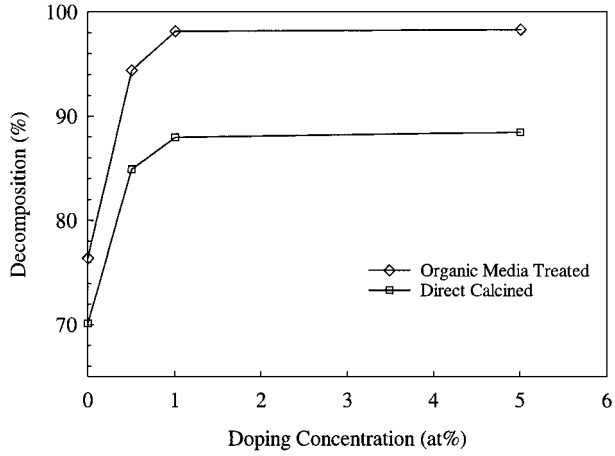

Figure 5 Photocatalytic activity of the Sb-doped TiO_2 as a function of doping concentration and preparation method. All the catalysts were calcined at 500°C for 2 h. Irradiation time was 42 min.

although the existence of such a phase was not detected by XRD.

Fig. 5 presents the influence of the synthesis procedure on the photocatalytic decomposition of MB over the various catalysts calcined at 500°C, 2 h. The detailed particle characteristics of each catalyst are listed in Table II. All the organic solvent treated catalysts exhibited better photocatalytic activity than the untreated counterparts. This improvement can mainly be attributed to the significant increase in surface area by the post-treatment, despite of a little less crystallinity. The undoped TiO_2 post-treated in the organic solvent decomposed 76.4% of MB, while 70.1% was observed for the directly calcined undoped TiO_2. For the 1 at% Sb-doped TiO_2, the photodecomposed amount of MB after 42 min irradiation was 98.2% over the organic solvent treated catalyst, and 88.0% for the untreated counterpart.

Studying the influence of the calcination conditions also reveals the importance of the catalyst particle characteristics in the photocatalytic activity. Fig. 6 presents the results of the photocatalytic degradation experiments over the organic solvent post-treated 5 at% Sb-doped TiO_2 samples calcined at different conditions. The detailed particle properties used in this study are summarized in Table III. Fig. 7 is the corresponding X-ray diffraction pattern showing the anatase-to-rutile phase transition behavior as a function of calcination temperature.

The optimum calcination temperature and time yielding the best catalytic activity were determined to be 500°C and 2 h. Surface area significantly decreased with

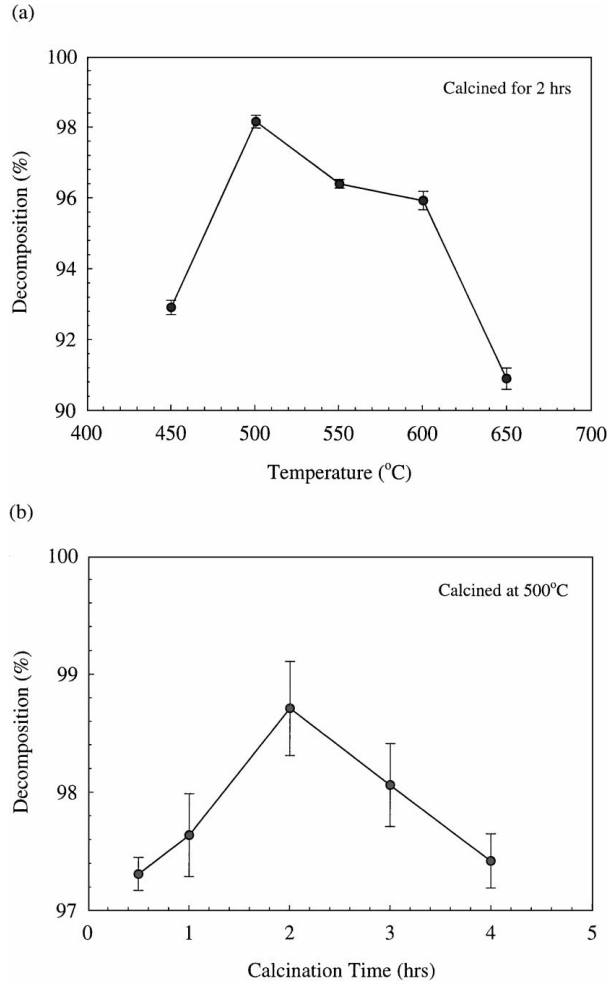

Figure 6 Photocatalytic activity of the organic solvent treated 5 at% Sb-doped TiO_2 as a function of (a) calcination temperature and (b) calcination time.

increasing calcination temperature from 166.7 m^2/g at 450°C to 76.0 m^2/g at 650°C. The estimated crystal size was also a strong function of the calcination temperature varying from 7.9 to 14.8 nm. Such microstructural variations directly influenced the photodegradation of MB. The sample calcined at 450°C, 2 h was less active toward the photodegradation of MB due to its poor crystallinity in spite of a high surface area. The photoactivity was maximized for the sample calcined at 500°C, which presented relatively well-crystallinity and high surface area. A further increase in the calcination temperature slightly enhanced the X-ray intensity of anatase. At the same time, however, the surface area of the catalyst rapidly decreased via particle growth,

TABLE III Particle characteristics and photocatalytic activity of the 5 at% Sb-doped TiO_2 powders submitted to different calcination temperatures

Calcination temperature (°C)	$I_{(Anatase)}/I_{Si}$	$I_{(Rutile)}/I_{Si}$	Fraction of rutile	Crystallite size (nm)	Surface area (m^2/g)	Decomposed MB (%)
450	0.80	0	0	7.88	166.7	92.9
500	1.21	0	0	8.48	149.2	98.2
550	1.30	0	0	9.97	131.5	96.4
600	1.43	0	0	9.98	110.8	95.9
650	1.67	0.76	0.36	14.84	76.0	90.9

All samples were post-treated in a butanol at 100°C followed by calcination at 500°C, 2 h.

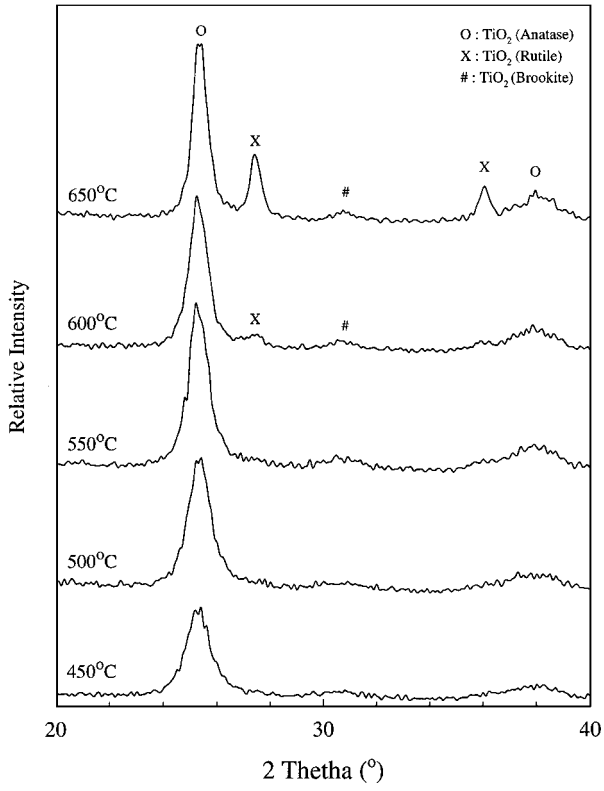

Figure 7 Variations in X-ray diffraction patterns for the organic solvent treated 5 at% Sb-doped TiO_2 as a function of calcination temperature. The samples were calcined for 2 h at each calcination temperature.

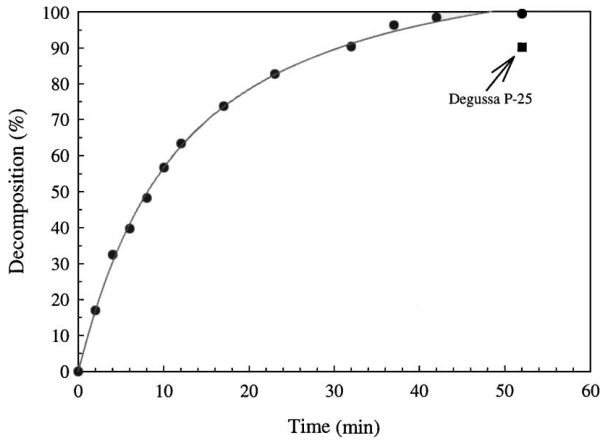

Figure 8 Photodecomposition of methylene blue by the organic solvent treated 5% Sb-doped TiO_2 as a function of irradiation time.

which became a dominating factor for lowering the net catalytic behavior. Decreased photoactivity for the catalyst calcined at 650°C may result from a significant reduction in the surface area in conjunction with the presence of the less photocatalytic active rutile and brookite phases.

Fig. 8 shows the extent of MB photodecomposition as a function of the irradiation time over the organic solvent treated 5 at% Sb-doped TiO_2. The decomposition occurred rapidly at the early stages of the reaction followed by a decrease at the later stages. The Sb-doped TiO_2 completely decomposed 100 ppm of MB within 1 hr, which was 9% better than the commercial Degussa P-25 under the same experimental conditions.

4. Discussion

Photocatalysis of TiO_2 is a complex function of the physical characteristics of the particles. Different preparation methods may result in different defect structures and surface morphologies, affecting the photoactivity. Doping with foreign cations further augments the complexity in understanding the photocatalytic process. The relative efficiency of a metal ion dopant depends on whether it serves as a mediator of interfacial charge transfer or as a recombination center. The ability of the dopant to function well is related to the dopant concentration, the energy level of the dopant within the TiO_2 lattice, its d electronic configuration, the distribution of the dopant within the particles [7, 19].

Although the exact understandings of the Sb-doping are still unclear in the current set of experiments, it is believed that Sb doping plays an effective shallow trap for charge carriers. For the photocatalytic decomposition of methylene blue by TiO_2, it was proposed that the surface-bound hydroxyl radical is the principal reactive oxidant [20]. Hydroxyl radicals are formed on the surface of TiO_2 by the reaction of holes in the valence band with adsorbed H_2O, hydroxide, or surface titanol group (=Ti-OH) [21–24]. A hydrogen atom is extracted from organic dye via hydroxyl radical attack. In this case, oxygen plays an important role as a primary electron acceptor and it should be supplied on continuous basis [22].

It seems that Sb dopant acts as electron traps retarding electron-hole recombination and enhancing interfacial hole transfer to degrade the organic dye adsorbed on the surface of the particles. When the dopant concentration is too high, however, the recombination rate will increase because the distance between trapping sites in a particle decreases with the number of dopants.

The Sb doping is also responsible for the red shift of the intrinsic absorption edge of TiO_2 and for the enhancement of the light absorption in the visible range as indicated by the DRS results in Fig. 3. Increased light absorption will allow energy transitions in the visible region in addition to the band gap transition in the near UV region, which possibly leads to a better photocatalytic efficiency.

However, the doping effect alone is not sufficient for explaining all the photocatalytic results in the present study. It is believed that the microstructural aspects of the catalysts play a significant role in determining the photocatalysis of methylene blue. Furthermore, the doping itself modifies the microstructural characteristics of the resulting doped catalysts. This correlation between the doping and the microstructural characteristics makes the photocatalytic behavior more complicated.

The dependence of MB decomposition with the doping content as shown in Fig. 4 can manifest such interrelationships between both parameters. The detailed Sb-TiO_2 catalyst characteristics used in this experiment are summarized in Table IV. The photocatalytic activity rapidly improves as the doping concentration increases and then reaches a plateau in the concentration range of 1–5 at%. Further doping above 5 at% makes the catalytic reactivity decreased. This photocatalytic

TABLE IV Particle characteristics and photocatalytic activity of the Sb-TiO_2 samples with various doping levels

Sb doping content (at%)	$I_{(Anatase)}/I_{Si}$	Crystallite size (nm)	Surface area (m^2/g)	Decomposed MB (%)
0.5	1.92	16.91	65.3	82.2
1	2.18	16.32	68.6	85.9
2	2.34	14.83	71.6	84.5
3	1.78	13.40	81.1	86.4
5	1.72	13.58	82.2	87.9
6	1.90	12.86	84.5	83.3
10	1.31	12.00	83.4	75.3

All samples were directly calcined at 600°C, 2 h without the organic solvent post-treatment.

behavior as a function of the doping content can be explained by dividing into three regimes.

The first would be the beneficial doping effect dominant regime in which the photocatalytic activity improves with the increasing doping content by effective charge carrier pair separation. The second regime can be characterized by a competition between the doping effect and the microstructural influence. An increase in the photoactivity by doping reaches a maximum at a concentration of 1 at%, beyond which the photocatalysis should decrease due to an increased charge carrier recombination. But the observed photoactivity is still high. The microstructural aspects come to play at this point since the catalyst characteristics vary with the increasing doping content as shown in Table IV. The relatively higher crystallinity of the anatase phase for the 2 at% Sb-TiO_2 may keep the catalyst still photoactive. Decreased particle size and increased surface area when the doping level is 3–5 at% may also compensate for the adverse doping effect. It is considered that such concurrent microstructural variation associated with the doping permits the Sb-doped TiO_2 to exhibit relatively high photoactivity over a wide range of doping levels. The final ragime shows the adverse doping effect dominance. The increasing doping content does not cause any observable variation in the microstructural characteristics above 6 at%. The excess doping thus significantly reduces the catalytic performance beyond the microstructural contribution, making the net photocatalytic activity to decrease.

5. Conclusions

Nanocrystalline doped TiO_2 photocatalysts have been synthesized by a coprecipitation method. Photocatalytic characterization in conjunction with microstructural evidence indicated that the photooxidation of methylene blue was a complex function of the dopant type and its concentration, and the particle characteristics of the catalysts. The Sb-doped TiO_2 exhibited better photocatalytic performance than the undoped TiO_2. Superior catalytic activity was observed in the Sb-doped TiO_2 at a doping concentration ranging from 1 to 5 at%. Using the 5 at% Sb-doped TiO_2 treated in butanol, 100 ppm of MB could be decomposed completely within 1 h, which was better than the commercial Degussa P-25. High photoactivity over a relative wide range of doping level is believed to result from interrelated contributions between a doping effect and the microstructural characteristics of the doped catalysts. When the doping is above the optimal concentration (∼1 at%), the photocatalytic activity should be deteriorated. However, the concurrent microstructural variation of the catalysts occurred with increasing doping concentration. This compensates to some extent for the adverse effect of the excess doping in the range of 1–5 at%. Above 5 at% Sb doping, however, accumulation of excess electrons significantly reduces the photocatalytic activity beyond the microstructural compensation.

References

1. A. L. LINSEBIGLER, G. LU and J. T. YATES JR., *Chem. Rev*. **95** (1995) 735.
2. P. V. KAMAT, *ibid*. **93** (1993) 267.
3. M. R. HOFFMANN, S. T. MARTIN, W. CHOI and D. W. BAHNEMANN, *ibid*. **95** (1995) 69.
4. Z. ZHANG, C.-C. WANG, R. ZAKARIA and J. Y. YING, *J. Phys. Chem*. **B102** (1998) 10871.
5. M. I. LITTER and J. A. NAVÍO, *J. Photochem. Photobiology* **A98** (1996) 171.
6. K. E. KARAKITSOU and X. E. VERYKIOS, *J. Phys. Chem*. **97** (1993) 1184.
7. W. CHOI, A. TERMIN and M. R. HOFFMANN, *ibid*. **98** (1994) 13669.
8. E. BORGARELLO, J. KIWI, E. PELIZZETTI, M. VISCA and M. GRÄTZEL, *J. Amer. Chem. Soc*. **103** (1991) 6324.
9. X. FU, L. A. CLARK, Q. YANG and M. A. ANDERSON, *Environ. Sci. Technol*. **30** (1996) 647.
10. R. BICKLEY, T. GONZALEZ-CARREÑO, A. R. GONZALEZ-ELIPÉ, G. MURUERA and L. PALMISANO, *J. Chem. Soc. Faraday Trans*. **90** (1994) 2257.
11. J. SORIA, J. C. CONESA, V. AUGUGLIARO, L. PALMISANO, M. SCHIAVELLO and A. SCLAFANI, *J. Phys. Chem*. **95** (1991) 274.
12. S. T. MARTIN, C. L. MORRISON and M. R. HOFFMANN, *ibid*. **98** (1994) 13695.
13. J. LIN, J. C. YU, D. LO and S. K. LAM, *J. Catalysis* **183** (1999) 368.
14. Y. R. DO, W. LEE, K. DWIGHT and A. WOLD, *J. Solid. State Chem*. **108** (1994) 198.
15. G. P. FOTOU, S. VEMURY and S. E. PRATSINIS, *Chem. Ing. Sci*. **49** (1994) 4939.
16. C. K. CHAN, J. F. PORTER, Y.-G. LI, W. GUO and C.-M. CHAN, *J. Amer. Ceram. Soc*. **82** (1999) 566.
17. A. P. RIVERA, K. TANAKA and T. HISANAGA, *Appl. Catal*. **B3** (1993) 37.
18. S. NASKAR, S. A. PILLAY and M. CHANDA, *J. Photochem. Photobiology* **A113** (1998) 257.
19. A. J. NOZIK and R. MEMMING, *J. Phys. Chem*. **100** (1996) 13061.
20. O. M. ALFANO, M. I. CABRERA and A. E. CASSANO, *J. Catal*. **172** (1997) 370.
21. S.-K. LEE, P. K. J. ROBERTSON, A. MILLS and D. MCSTAY, *J. Photochem. Photobiology* **A122** (1999) 69.
22. N. XU, Z. SHI, Y. FAN, J. DONG, J. SHI and M. Z.-C. HU, *Ind. Eng. Chem. Res*. **38** (1999) 373.
23. R. W. MATTHEWS, *J. Chem. Soc. Faraday Trans*. **85** (1989) 1291.
24. P. REEVES, R. OHLHAUSEN, D. SLOAN, K. PAMPLIN, T. SCOGGINS, C. CLARK, B. HUTCHINSON and D. GREEN, *Solar Energy* **48** (1992) 413.

Received 24 November 1999
and accepted 6 July 2000